

pyaneti: a fast and powerful software suite for multi-planet radial velocity and transit fitting

O. Barragán,^{1*} D. Gandolfi,¹ and G. Antoniciello^{1,2}

¹*Dipartimento di Fisica, Università di Torino, via P. Giuria 1, 10125 Torino, Italy*

²*Dipartimento di Fisica e Astronomia “Galileo Galilei”, Università di Padova, Vicolo dell’Osservatorio 3, 35122 Padova, Italy*

Accepted XXX. Received YYY; in original form ZZZ

ABSTRACT

Transiting exoplanet parameter estimation from time-series photometry and Doppler spectroscopy is fundamental to study planets’ internal structures and compositions. Here we present the code `pyaneti`, a powerful and user-friendly software suite to perform multi-planet radial velocity and transit data fitting. The code uses a Bayesian approach combined with an MCMC sampling to estimate the parameters of planetary systems. We combine the numerical efficiency of FORTRAN, the versatility of PYTHON, and the parallelization of OpenMP to make `pyaneti` a fast and easy to use code. The package is freely available at <https://github.com/oscaribv/pyaneti>.

Key words: methods: numerical – planets and satellites: general – techniques: photometry – techniques: spectroscopy

1 INTRODUCTION

A new branch of astrophysics was born with the discovery of the first planet orbiting a star other than the Sun (Mayor & Queloz 1995). Since then, astronomers have developed new techniques to detect and characterize exoplanets (Seager 2010; Perryman 2011). The two more successful techniques are the transit and radial velocity (RV) methods (see, e.g., Bozza et al. 2016). They provide a direct measurement of the planet radius (Charbonneau et al. 2000; Henry et al. 1999) and minimum mass (Mayor & Queloz 1995), respectively. By combining transit photometry with RV measurements, it is possible to measure the true mass and determine the planetary mean density. This allows us to study planets’ internal structure and composition and gives us important hints as to their formation and evolution.

The success of the transit method relies on both ground- (e.g., HAT-Net, KELT, WASP; Bakos et al. 2004; Pepper et al. 2007; Pollacco et al. 2006) and space-based photometric surveys (e.g., CoRoT, Kepler, and K2; Auvergne et al. 2009; Borucki et al. 2010; Howell et al. 2014), which have led to the discovery of more than 2800 transiting exoplanets¹. The RV method has strongly benefited from state-of-the-art high-precision ($\sim 1 \text{ m s}^{-1}$) spectrographs such as HIRES (Vogt et al. 1994), HARPS (Mayor et al. 2003), and HARPS-N (Cosentino et al. 2012), which have opened up the doors to the Earth-

mass domain. Future exoplanet surveys and follow-up observations conducted with both space-based (TESS, PLATO, CHEOPS; Ricker et al. 2015; Rauer et al. 2014; Broeg et al. 2013) and ground-based (e.g., ESPRESSO, SPIRou; Pepe et al. 2010; Donati et al. 2017) facilities will provide us with a wealth of photometric and spectroscopic time-series data sets that need powerful tools for a fast and robust analysis.

Radial velocity and transit light curves are described by time-dependent parametric equations. By comparing models with data we can determine the physical properties of planetary systems. Bayesian model fitting techniques, such as Markov chain Monte Carlo (MCMC) methods, are widely used for parameter estimation and their popularity among the astronomers’ community has steadily increased in the past two decades (see, e.g., Sharma 2017).

Markov chain Monte Carlo data analysis is a reliable statistical method to estimate planetary parameters. However, it can be computationally challenging, especially when the amount of data is large and the dimension of the parameter space that one needs to explore is high. Some examples of such cases include: long-cadence photometric data – as those collected by Kepler and K2 – for which the transit model has to be re-sampled to account for the long integration time (Kipping 2010); the light curve of stars hosting ultra-short-period transiting planets ($P < 1$ day), which includes hundreds or even thousands of transits (e.g., Gandolfi et al. 2017; Guenther et al. 2017; Sanchis-Ojeda et al. 2014); low-mass planets whose masses can be precisely derived only collect-

* E-mail: oscar.barraganvil@edu.unito.it

¹ As of July 2018, exoplanet.eu.

ing hundreds of RV data points (e.g., [Hatzes et al. 2011](#)); multi-planet systems whose parameter space increases dimensionality with the addition of each planet (e.g., [Gillon et al. 2017](#)). Combining sophisticated statistical methods and powerful numerical tools is therefore an optimal approach to simultaneously model photometric and RV data.

There is a variety of software packages in the literature that allow us to determine the physical parameters of exoplanets from time-series photometry and RV measurements, using either purely Bayesian approaches (e.g. `PYTRANSIT`, `PyTranSpot`; [Parviainen 2015](#); [Juvan et al. 2018](#)), or different methods (e.g. `TLMC` [Csizmadia et al. 2015](#)). Some of these packages can model transit light curves (`PYTRANSIT`; `PyTranSpot`), RV curves (e.g., `RVLIN`, [Wright & Howard 2009](#)), or even perform a joint analysis of the photometric and RV data (e.g., `TLMC`; `EXOFAST`, [Eastman et al. 2013](#)).

In this work we present the software suite `pyaneti`². This code is a new powerful tool to perform multi-planet fit to RV and/or transit data sets. It combines the MCMC technique with the computational power of `FORTRAN` and the versatility of `PYTHON`. This code has already been used for the analysis of several planetary systems (see, e.g., [Barragán et al. 2016, 2018a,b](#); [Chakraborty et al. 2018](#); [Fridlund et al. 2017](#); [Gandolfi et al. 2017](#); [Guenther et al. 2017](#); [Li et al. 2017](#); [Livingston et al. 2018](#)).

The paper is organized as follows. For the sake of self-consistency, we provide a short recap of Bayesian analyses and MCMC algorithms in Sect. 2. The RV and transit equations used by `pyaneti` are given in Sect. 3. Section 4 describes the general algorithms used by the code. We test the package in Sect. 5 and conclude in Sect. 6.

2 MATHEMATICAL APPROACH

2.1 The Bayes' theorem

The aim of data analysis is to extract information from experiments and/or observations. In this work, we are interested in extracting planetary physical parameters by comparing parametric models with astronomical observations. From a probabilistic point of view, we want to estimate the probability that a physical parametric model $M = M(\vec{\phi})$, function of some parameters $\vec{\phi}$, describes the data D . Such probability is called the conditional probability of M given D and it can be written as $P(M|D)$.

Bayes' theorem ([Bayes & Price 1763](#)) provides a simple and robust mathematical framework to compute $P(M|D)$ as

$$P(M|D) = \frac{P(D|M)P(M)}{P(D)}. \quad (1)$$

In a context of a fixed dataset, $P(D|M)$ is a function of the model called the likelihood of observing the data set D if the model M is true, while $P(M)$ is the prior probability associated to the model M , and $P(D)$ is the model evidence. $P(M|D)$ is called the joint posterior distribution and it gives the probability that a model M is true given D is true.

2.2 Likelihood

For a given data set D composed of N measurements $D_{1,\dots,N}$, we can generate a set of N predicted points $M_{1,\dots,N}$ from a parametric model. The likelihood of a point D_i being described by a point M_i is written as $P(D_i|M_i)$. The likelihood of the whole data set D to be described by the model M is given by the product of each probability $P(D_i|M_i)$ as

$$P(D|M) = \prod_{i=1}^N P(D_i|M_i). \quad (2)$$

In order to compute $P(D|M)$ using eq. (2), we need to find out which likelihood functions describes better our data. If we assume that our measurements are normally distributed, independent, and that only contain uncorrelated noise σ_i , the likelihood of the data point D_i being true, assuming M_i is also true, is written as

$$P(D_i|M_i) = \frac{1}{\sqrt{2\pi(\sigma_i^2 + \sigma_j^2)}} \exp\left\{-\frac{1}{2} \frac{(D_i - M_i)^2}{\sigma_i^2 + \sigma_j^2}\right\}, \quad (3)$$

where the terms σ_j are used to normalize the likelihood in the case the nominal uncertainties σ_i are underestimated (see e.g., [Sharma 2017](#)). If we use eq. (3) for a data set, its likelihood is given by using eq. (2) as

$$P(D_i|M_i) = \prod_{i=1}^N \left[\frac{1}{\sqrt{2\pi(\sigma_i^2 + \sigma_j^2)}} \right] \exp\left\{-\frac{1}{2} \chi^2\right\}, \quad (4)$$

where

$$\chi^2 = \sum_{i=1}^N \frac{(D_i - M_i)^2}{\sigma_i^2 + \sigma_j^2}. \quad (5)$$

`pyaneti` uses the likelihood given by eq. (4), but we acknowledge that more general likelihoods exist, in which possible correlated noise between data points is taken into account (see, e.g., [Parviainen 2017](#); [Sharma 2017](#)). We also note that for numerical reasons, it is better to treat $P(M|D)$ in a logarithmic way ([Appendix A](#)).

2.2.1 Priors

Priors contain previously known information about a given model parameter, e.g., some physical range in which a parameter has equal probability to lie. Alternatively, the parameter's probability can be given by a distribution based on previous estimates. Widely used priors are the uniform and Gaussian priors.

A *uniform prior* is called a weakly informative or uninformative prior. It is used when the only available information about a given parameter ϕ_i is that it lies inside a range $[a, b]$. For example, we know that the eccentricity of an elliptical orbit ranges between 0 and 1. If the parameter ϕ_i lies between a and b with equal probability, its uniform prior is given by

$$\mathcal{U}(\phi_i; a, b) = \begin{cases} (b-a)^{-1} & : a < \phi_i < b \\ 0 & : \text{otherwise} \end{cases} \quad (6)$$

² From the Italian word *planeti*, which means *planets*.

A *Gaussian prior* is called an informative prior. This prior is useful when, for a given parameter, we have a previous measurement and its $1\text{-}\sigma$ uncertainty, and we want to use this information to weight the probability. For instance, if we have asteroseismology-derived mass and radius of a star hosting a transiting planet, we can use these quantities together with the orbital period to set a Gaussian prior on the semi-major axis of the planet’s orbit through Kepler third law.

A Gaussian prior of a given parameter ϕ_i with median a and standard deviation b is given as

$$\mathcal{N}(\phi_i; a, b) = \frac{1}{\sqrt{2\pi b^2}} \exp\left[-\frac{(\phi_i - a)^2}{2b^2}\right]. \quad (7)$$

In this work we describe only the uniform and Gaussian priors, as those are currently implemented in `pyaneti`. We acknowledge the existence of other priors in the literature (see, e.g., [Díaz 2018](#); [Sharma 2017](#)). Figure 1 shows how priors can affect the final posterior distribution for a fixed likelihood. For instance, the upper and lower limits of a flat prior may truncate or exclude the maximum of the likelihood function. The influence of a Gaussian prior on the posterior distribution depends on the prior’s center and width, as well as on the number of data points (e.g., [Gelman et al. 2004](#)).

2.2.2 Model evidence

The term $P(D)$ in equation (1) is called model evidence or marginal likelihood. It has the function to normalize the posterior distribution. By definition $P(D)$ is calculated by integrating the likelihood and prior distributions in the parameter space as

$$P(D) = \int P(D|M(\vec{\phi}))P(M(\vec{\phi}))d\vec{\phi}. \quad (8)$$

2.2.3 Marginal posterior distribution

We now have a mathematical description of all the components to calculate $P(M|D)$ from equation (1). In order to derive the parameters, we are interested on the shape of the posterior distribution of each parameter ϕ_i more than in its normalized probability. The parameter estimation can be extracted from the non-normalized posterior distribution, i.e. the term $P(D|M)P(M)$, ignoring the evidence term $P(D)$. We note that the evidence term has an important role when doing Bayesian comparison between different models (see, e.g., [Gelman et al. 2004](#)).

Since M is a parametric model, we can marginalize the parameter ϕ_i by integrating $P(D|M)P(M)$ over the remaining $\phi_{j \neq i}$ parameters. This leads to a marginal posterior distribution for each parameter ϕ_i from which we can infer the model parameters.

2.3 Markov chain Monte Carlo

The calculation of a marginal posterior distribution can be done analytically or numerically. However, in some cases it may not have an analytic solution. For instance, numerical iterative methods are widely used to sample the parameter

space in order to generate marginal posterior distributions from a collection of data points.

An efficient method to generate a set of data points in a parameter space is by using a *Markov chain*. Following the definition of [Sharma \(2017\)](#), a Markov chain is a sequence of random variables X_1, \dots, X_n such that, given the present state, the future and past are independent. If random numbers are used to generate the Markov chains, this method is called Markov chain Monte Carlo (MCMC). These random variables can be the points $\vec{\phi}$ in the parameter space that we want to sample. For instance, if we start a point in the parameter space $\vec{\phi}_1$, we can generate a set of different models $\vec{\phi}_i$ via Markov chains. In this way, we can create a set of N models from an initial $\vec{\phi}_1$.

There is a large variety of MCMC sampling methods, which ensure that the Markov chains converge to the optimal solution where the posterior has a static solution. For a basic MCMC algorithm, we refer the reader to the Metropolis-Hastings algorithm ([Metropolis et al. 1953](#); [Hastings 1970](#)). In the next section we will describe the ensemble sampler algorithm ([Goodman & Weare 2010](#)) that is used by `pyaneti` for the parameter estimations. This algorithm was first used by [Hou et al. \(2012\)](#) to infer parameters from time-series RV measurements.

2.4 Ensemble sampler algorithm

The *ensemble sampler* algorithm uses a group of Markov chains to explore the parameter space. Each chain j starts with a point in the parameter space $\vec{\phi}_{j,t}$ and is evolved using the complementary chains of the ensemble.

[Christen \(2007\)](#) found that it is possible to evolve the chain $\phi_{j,t}$ to the state $t + 1$ via a *walk move* using a complementary chain of the ensemble. [Goodman & Weare \(2010\)](#) used the idea of the walk move to construct an affine invariant move called *stretch move*. The stretch move for the chain $\vec{\phi}_{j,t}$ is defined as

$$\vec{\Phi}_j = \vec{\phi}_{k,t} + z \left(\vec{\phi}_{j,t} - \vec{\phi}_{k,t} \right), \quad (9)$$

where $\vec{\phi}_{k,t}$ is a complementary chain of the ensemble, such that $j \neq k$ and z is a scaling variable that regulates the step. This scaling variable has to come from a density distribution g with the symmetry condition ([Christen 2007](#))

$$g\left(\frac{1}{z}\right) = z g(z). \quad (10)$$

A distribution that follows this condition is

$$g(z) \propto \begin{cases} \frac{1}{\sqrt{z}} & : z \in \left[\frac{1}{a}, a\right] \\ 0 & : \text{otherwise,} \end{cases} \quad (11)$$

where $a > 1$. There is no optimal value for a , but we set $a = 2$ to be consistent with ensemble sampler algorithms in the literature (e.g., [Goodman & Weare 2010](#); [Hou et al. 2012](#)). To ensure the invariant distribution we have to compute the ratio

$$q = z^{N-1} \frac{P(M(\vec{\Phi})|D)}{P(M(\vec{\phi}_{j,t})|D)}. \quad (12)$$

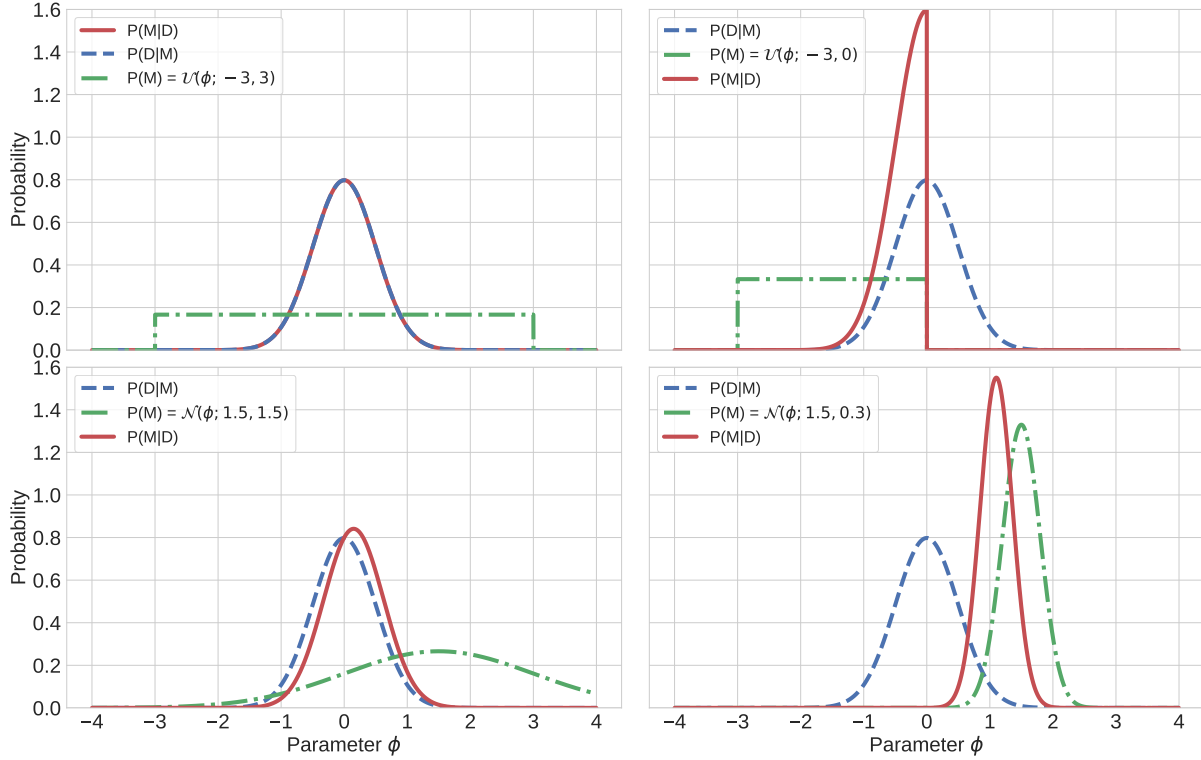


Figure 1. Posterior distributions (solid red line) for a fixed likelihood (blue dashed lines) and different priors (green dot-dashed lines). All quantities have been normalized for comparison purpose. *Upper left:* Uniform prior with limits $[-3, 3]$. *Upper right:* Uniform prior with limits $[-3, 0]$. *Lower left:* Gaussian prior with mean 1.5 and standard deviation 1.5. *Lower right:* Gaussian prior with mean 1.5 and standard deviation 0.3.

The term z^{N-1} ensures detailed balance (for more details see [Goodman & Weare 2010](#)). To decide whether we accept or not the proposed state we use

$$\begin{aligned} \vec{\phi}_{j,t+1} &= \vec{\Phi}_j & : q > U \\ \vec{\phi}_{j,t+1} &= \vec{\phi}_{j,t} & : q \leq U, \end{aligned} \quad (13)$$

where U is a random number between $[0, 1]$. After a number N of iterations and L chains, we will have $N \times L$ samples for each parameter from which we can create posterior distributions. A general overview of a single step of the ensemble sampler method is given in [Algorithm 1](#).

[Figure 2](#) shows an example of the evolution of an ensemble sampler algorithm using six chains. The latter start at a different point in the parameter space. After a finite number of iterations (in this case a few hundreds), the chains converges to a stable region of the parameter space. Details on how we create marginal posterior distributions from chain’s samples are provided in [Section 2.6](#).

Another advantage of this approach is that, since each Markov chain evolves independently, this algorithm can be parallelized ([Foreman-Mackey et al. 2013](#)).

2.5 Convergence

In order to infer the parameter values based on a MCMC sampling we need to use chains that have converged. A widely used convergence test has been developed by [Gelman & Rubin \(1992\)](#). This test compares the “between-chain” B

input : Initial ensemble of N states $\vec{\phi}_{j,t}$
output: Ensemble of N states $\vec{\phi}_{j,t+1}$

- 1 **for** $j = 1$ **to** N **do**
- 2 Select a complementary state from the ensemble such that $j \neq k$
- 3 Sample the scaled variable z from the density distribution g
- 4 Propose the new state via a walk move
 $\vec{\Phi}_j = \vec{\phi}_{k,t} + z(\vec{\phi}_{j,t} - \vec{\phi}_{k,t})$
- 5 Compute q from eq. (12) using likelihood and priors for the states $\vec{\phi}_{j,t}$ and $\vec{\Phi}_j$
- 6 Sample a uniform random variable U between 0 and 1
- 7 **if** $q > U$ **then**
- 8 $\vec{\phi}_{j,t+1} = \vec{\Phi}_j$
- 9 **else**
- 10 $\vec{\phi}_{j,t+1} = \vec{\phi}_{j,t}$
- 11 **end**
- 12 **end**

Algorithm 1: One iterations of the ensemble sampler algorithm.

and “within-chain” W variance via the scaled potential factor $\hat{R} = \sqrt{[W(n-1)/n + B/n]/W}$, where n is the length of each chain. We define convergence as when chains have $\hat{R} < 1.02$ for all the parameters ([Gelman et al. 2004](#)).

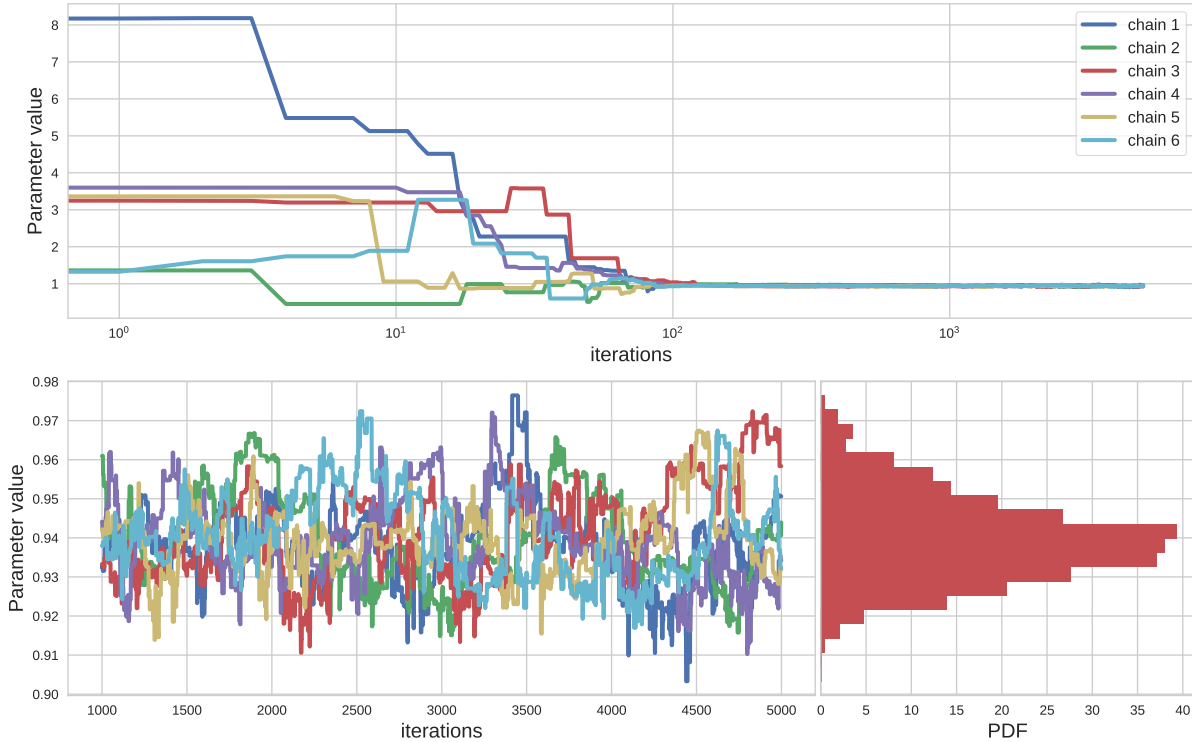


Figure 2. Example of the evolution of an ensemble sampler algorithm using six chains. *Upper panel:* Parameter value for each chain from iteration 0 to 5000 in logarithmic scale. *Lower left panel:* Chains behavior for the last 4000 iterations. *Lower right panel:* Histogram created using the information contained in all the chains in the last 4000 iterations.

2.6 Marginal posterior distribution from parameter sampling

Chains that have converged to a static solution represent a sample of the marginal posterior distribution from which they were sampled. The frequencies of the chains can be used to create the posterior distribution of the sampled parameters. A common way to draw the sampling frequency is with a histogram, as shown in Fig. 2. The final marginal posterior distribution for each parameter is also called *credible interval*.

The median and the 68% limits of the credible interval are commonly used to define the parameter’s best estimate and its uncertainty (see, e.g., Hogg & Foreman-Mackey 2018). When the marginal posterior distribution follows a Gaussian distribution, the median and the 68% limits of the credible interval correspond to the mean and standard deviation of a normal distribution. When the posterior distribution is skewed, the 68% limits are not symmetric with respect to the median, and they give an “first-order” idea of the shape of the marginal posterior distribution that describes a given parameter.

3 MULTI-PLANET EQUATIONS

In this section, we describe the equations used by `pyaneti` to extract parameter values from time-series RV and photometric transit data. For a detailed derivation of the equations presented in the following sub-sections, we refer the reader

to the specific literature (see, e.g., Murray & Correia 2010; Winn 2010).

3.1 Radial velocity equations

The motion of a planet orbiting a star can be reduced to a two-body problem in which one of the two body is far more massive than the other. The change of the velocity component along the line-of-sight to the host star, induced by the presence of the orbiting planet, is described by the following equation

$$f_{\text{RV}}(\vec{\phi}; t) = \gamma + K_{\star} [\cos(\theta + \omega_{\star}) + e \cos \omega_{\star}], \quad (14)$$

where γ is the systemic velocity of the center of mass, θ is the true anomaly, e the orbital eccentricity, and ω_{\star} the angle of periastron of the star. K_{\star} is the radial velocity semi-amplitude variation, which is given by

$$K_{\star} = \left(\frac{2\pi G}{P} \right)^{1/3} \frac{M_{\text{p}} \sin i}{(M_{\text{p}} + M_{\star})^{2/3}} \frac{1}{(1 - e^2)^{1/2}}, \quad (15)$$

Equation (15) provides a relation between the semi-amplitude RV variation of the star K_{\star} and the planetary M_{p} and stellar mass M_{\star} . The remaining parameters of eq. (15) are the gravitational constant G (we use the IAU units given by Prša et al. 2016), the orbit inclination with respect to the line-of-sight i , and the orbital period P . Since $M_{\text{p}} \ll M_{\star}$, we can assume that $(M_{\text{p}} + M_{\star})^{2/3} \approx M_{\star}^{2/3}$. The dependence on the orbit inclination implies that only the planet’s minimum

mass $M_p \sin i$ can be measured, provided that the stellar mass M_\star is known. In order to determine the planet's true mass, the orbit inclination has to be measured. For transiting exoplanets, the inclination can be derived from the modeling of the transit light curve (Sect. 3.2).

The time dependency of θ is given by

$$\theta(t) = 2 \arctan \left[\sqrt{\frac{1+e}{1-e}} \tan \left(\frac{E(t)}{2} \right) \right] \quad (16)$$

where the eccentric anomaly $E(t)$ is defined via

$$A(t) = E(t) - e \sin[E(t)] \quad (17)$$

and where

$$A(t) = \frac{2\pi}{P} (t - T_p) \quad (18)$$

is the mean anomaly. The latter depends on time t and on a zero point T_p , which is the time of passage of periastron. We stress that we fit for the time of minimum conjunction of the planet T_0 that, for transiting planets, coincides with the time of transit. It is straightforward to pass from T_0 and T_p since the corresponding points in the planet's orbit are separated by an angle of $\pi/2 - \omega_\star$. We note that eq. (17) is transcendental and cannot be solved analytically with respect to the eccentric anomaly $E(t)$. `pyaneti` solves eq. (17) using a Newton-Raphson algorithm.

If a star is orbited by N_p planets – which we assume their mutual gravitational interaction is negligible – the general expression for eq. (14) is then

$$M_{\text{RV}}(\vec{\phi}; t) = \gamma_i + \sum_{j=1}^{N_p} K_j [\cos(\theta_j + \omega_{\star,j}) + e_j \cos \omega_{\star,j}]. \quad (19)$$

The term γ_i depends on the spectrograph i to account for possible instrumental offsets. Equation (19) can be modified to add linear or quadratic acceleration terms that may be present in the data.

The general parametric function $M_{\text{RV}}(\vec{\phi}; t)$, which describes the Doppler reflex motion of a star orbited by more than one planet is then

$$M_{\text{RV}}(\vec{\phi}; t) = f(\{T_0, P, e, \omega_\star, K\}_j, \gamma_i; t), \quad (20)$$

in which the set of parameters $\{T_0, P, e, \omega_\star, K\}$ repeats for each planet j and γ_i accounts for each different instrument i .

3.2 Transit equations

An eclipse occurs when an astronomical body is obscured by a second one. A transit is a special case of eclipse, in which a smaller object passes in front of a larger body. If the orbit inclination is close to 90° , the presence of a planet orbiting its host star can be inferred by detecting the periodic drops of stellar flux caused by the planet partly occulting the stellar disk. The fraction of light occulted by a planet during a transit is proportional to its size, being about 1% for a Jupiter-size object and 100 times smaller for an Earth-size planet transiting a Solar-like star.

An useful quantity to describe a planetary transit is the scaled projected distance between the planet's and the star's center defined as (see, e.g., [Winn 2010](#))

$$\delta = \frac{a}{R_\star} \frac{(1-e^2)}{(1+e \cos \theta(t))} \sqrt{1 - \sin^2(\theta(t) + \omega_\star) \sin^2 i}, \quad (21)$$

where a is the semi-major axis of the relative orbit³, R_\star is the stellar radius, and the remaining parameters are the same used in the RV equations presented in Sect. 3.1. We note that δ depends on the true anomaly $\theta(t)$, which in turn is a function of time according to eqs. (16), (17) and (18). Following [Eastman et al. \(2013\)](#), we define the projected distance δ using the argument of periastron of the star ω_\star instead of the argument of periastron of the planet ω_p . If we define $r_p \equiv R_p/R_\star$ as the planet-to-star radius ratio, from equation (21), the transit of an exoplanet occurs only when $\delta < 1 + r_p$ and $\sin(\theta(t) + \omega_\star) > 0$ (star behind the planet). On the other hand, the planet's occultation – also known as secondary eclipse – occurs if $\delta < 1 - r_p$ and $\sin(\theta(t) + \omega_\star) < 0$ (planet behind the star).

In order to analytically describe how the total flux $F(t)$ changes as a function of time due to the presence of a transiting planet, we need to account for the disk-integrated stellar flux $F_\star(t)$, the planet flux $F_p(t)$ (both reflected light and thermal emission), and the loss of light when transits/occultations occur $\lambda(\delta, r_p)$. The total flux $F(t)$ is given by

$$F(t) = F_\star(t) + F_p(t) - \lambda(\delta, r_p). \quad (22)$$

We assume that the stellar flux $F_\star(t)$ is constant and equal to 1, and that any variation can be expressed as a fraction of the stellar light. We also assume that the planet contribution to the light curve is negligible ($F_p = 0$), i.e., we assume that occultations and phase curve have no effect on the observed light curve. Under these assumptions, eq. (22) can be re-written as

$$F(t) = 1 - \lambda(\delta, r_p). \quad (23)$$

By definition $\lambda = 0$ when $\delta > 1 + r_p$. For cases where $\delta < 1 + r_p$, the change of light depends on the analytical form of λ , which accounts for the loss of light as the planet crosses the stellar disk. There are different approaches to define the analytical form of $\lambda(\delta, r_p)$. The simplest approach is to assume that the stellar disk is a uniform source of light ([Seager & Mallén-Ornelas 2003](#)). However, real stellar disks are brighter in the center and fainter at the edge (the limb), a phenomenon known as limb darkening (see, e.g., [Claret & Bloemen 2011](#)). `pyaneti` uses the [Mandel & Agol \(2002\)](#)'s transit light curve model in which the stellar intensity is limb-darkened using a quadratic law with coefficients u_1 and u_2 . [Mandel & Agol \(2002\)](#) provide the function $\lambda(\delta, r_p)$ for a single planet transiting a star.

³ The semi-major axis of the relative orbit is defined as $a = a_p + a_\star$, where a_p and a_\star are respectively the semi-major axes of the planet's and star's orbit with respect to the center of mass.

For a system where there are N_p transiting planets, the relative flux of the star is then

$$F(t) = 1 - \sum_{j=1}^{N_p} \lambda_j(\delta, r_p). \quad (24)$$

According to eq. (24), $F(t) = 1$ if no planet transits the star; it reduces to the one-transiting-planet case when there is a single planet crossing the stellar disk. Equation (24) takes also into account multi-planet transit events. We note that this approach does not take into account occultations between planets that may occur.

The general parametric function $M_{tr}(\vec{\phi})$ that describes transit events in a light curve is

$$M_{tr}(\vec{\phi}; t) = f(\{T_0, P, e, w_\star, R_p/R_\star, a/R_\star, i\}_j, \{u_1, u_2\}_i; t). \quad (25)$$

The set of parameters $\{T_0, P, e, w_\star, R_p/R_\star, a/R_\star, i\}$ repeats for each planet j . Each $\{u_1, u_2\}$ repeats for each band i of the light curve.

3.3 Multi-planet joint fit

When both Doppler and transit data are available, the best approach to perform the analysis is via a joint fit. By comparing the RV and the transit equations (eqs. 20 and 25), we see that T_0 , P , e and w_\star are shared parameters. In this case the orbital parameters are fitted simultaneously. Usually, the transit light curves improve the determination of T_0 and P , whereas the RV measurements constrain better e and w_\star . The parameters involved in the joint fit are

$$\vec{\phi} = (\{T_0, P, e, w_\star, R_p/R_\star, a/R_\star, i, K\}_j, \{u_1, u_2\}_i, \gamma_k), \quad (26)$$

where $\{T_0, P, e, w_\star, R_p/R_\star, a/R_\star, i, K_\star\}_j$ repeats for each planet j , $\{u_1, u_2\}_i$ for each photometric band i , and γ_K for each spectrograph k .

3.4 Parametrizations

Equation (26) defines the general set of parameters that can be extracted by modeling RV measurements and transit photometry. It is possible to use a set of convenient parametrizations to improve the exploration of the parameter space and avoid biases due to priors. In the following sub-sections we provide a brief description of the parameterizations used by *pyaneti*.

3.4.1 Eccentricity and angle of periastron

The posterior distribution of the eccentricity is not well sampled for orbits with small eccentricities (Lucy & Sweeney 1971). A practical solution is to define e and w_\star using a polar form. *pyanety* adopts the parametrization proposed by Anderson et al. (2011)

$$ew_1 = \sqrt{e} \sin \omega_\star, \quad ew_2 = \sqrt{e} \cos \omega_\star. \quad (27)$$

This parameterization has two advantages: *a*) it is not truncated when the eccentricity is close to zero; *b*) uniform priors on ew_1 and ew_2 imply uniform priors on the eccentricity.

3.4.2 Impact factor

As presented in Sect. 3.2, the transit of a planet can be described using the scaled projected distance between the planet and star centers. It is then convenient to parametrize the stellar inclination using a parameter that takes into account the projected distance. A practical approach is via the impact parameter defined as (Winn 2010)

$$b = \frac{a}{R_\star} \cos i \left(\frac{1 - e^2}{1 + e \sin \omega_\star} \right). \quad (28)$$

The advantage of using the impact factor is that b can be compared directly with the projected distance z . In this way it is easy to set priors to exclude orbits for which there are no transit, i.e., when $b > 1 + r_p$.

3.4.3 Limb Darkening coefficients

For the limb darkening coefficients *pyaneti* uses the parameterization proposed by Kipping (2013), who showed that an optimal way to sample the parameter space for the Mandel & Agol (2002)'s limb darkening coefficients is via the parametrization

$$q_1 = (u_1 + u_2)^2, \quad q_2 = \frac{u_1}{2(u_1 + u_2)}. \quad (29)$$

The advantage of this approach is that it fully accounts for our ignorance about the intensity profile and explores physical solutions by sampling uniformly q_1 and q_2 between 0 and 1. This yields robust and realistic uncertainty estimates. It is possible to recover the original u_1 and u_2 coefficients via

$$u_1 = 2q_1 \sqrt{q_2}, \quad u_2 = \sqrt{q_1} (1 - 2q_2). \quad (30)$$

3.4.4 Stellar density

From Kepler's third law we obtain that

$$\rho_\star + r_p^3 \rho_p = \frac{3\pi}{GP^2} \left(\frac{a}{R_\star} \right)^3. \quad (31)$$

where ρ_\star is the star's mean density, ρ_p the planet's mean density, r_p the planet-to-star radius ratio, P the orbital period, R_\star the star's radius, and a the semi-major axis of the relative orbit. Since r_p^3 is relatively small, the second term of the left side of eq. (31) can be neglected (Winn 2010). There is thus a relation between the stellar density and the orbital parameters P and a/R_\star that can be used to compare stellar density derived from the modeling of the transit light curves with an independent determination (e.g., from spectroscopy).

It is convenient to parametrize a/R_\star with ρ_\star . If precise stellar parameters have been calculated, it is possible to set tight priors on the stellar density and hence on a/R_\star . For a multi-planet system, it is convenient to parameterize the scaled semi-major axis a_j/R_\star of all planets j using the same stellar density. In this way the stellar density is constrained for all planets and Kepler's third law is not violated within planets orbiting the same star.

`pyaneti` uses the parametrization $\rho_{\star}^{1/3}$ instead of ρ_{\star} because a/R_{\star} and $\rho_{\star}^{1/3}$ are linearly related assuming $r_p \approx 0$ (eq. 31).

4 CODE OVERVIEW

If we combine the MCMC analysis described in Sect. 2 along with the multi-planet equations presented in Sect. 3, we can develop a powerful tool to estimate planet parameters from Doppler and transit observations. We used this approach together with the computational speed of `FORTRAN` and the versatility of `PYTHON` to write the software suite `pyaneti`. The computation-demanding routines, such as orbital solutions, likelihood calculations, etc., are calculated by `FORTRAN` subroutines. The input and output routines, such as data preparation, plot creations, etc., are handled by `PYTHON`. `FORTRAN` subroutines are wrapped to `PYTHON` using `F2PY`⁴.

One of the main advantages of `pyaneti` is that all the code controls are given inside a `PYTHON`-based input file. Priors, fitted parameters, and data files are controlled via flags and python objects. This allows one to run the code with only one command line. A general overview of the algorithm of the code is given in Algorithm 2.

The advantage of using the ensemble sampler algorithm described in section 2.4 is that it can be parallelized. This speed-up the global solution of the MCMC run. The parallelization is done following the procedure described in Foreman-Mackey et al. (2013), in which we divide the ensemble in two subsamples and evolve each group taking a chain from the complementary set of chains. We use Open Multi-Processing (`OpenMP`) to perform the parallelization inside the `FORTRAN` routines.

There are some physical effects that are not included in the current version of the code. Transit timing variations (TTVs), mutual interaction between planets, multi-band photometry, Rossiter-McLaughlin effect, planet's occultations, planet's phase curve fitting have not been implemented yet. `pyaneti` currently uses likelihood and priors as described in Sect. 2. More general likelihoods, such as Gaussian Process, have not been included yet. Nevertheless, the code is written in a modular way making it easy and straightforward to implement additional physical effects or equations. We plan to keep maintaining and upgrading `pyaneti`.

5 CODE TESTS

5.1 A toy model

5.1.1 Setup

We created a set of synthetic RV and transit data to check the performance of `pyaneti`. The simulated planetary system includes three planets: the two innermost planets transit the star, whereas the outer planet can only be seen in the RV data set.

Synthetic data points were created assuming a star with a mass of $0.66 M_{\odot}$ and radius of $0.67 R_{\odot}$. The planets have

periods of 1.21321, 5.61122, and 12.12349 days with conjunction times of 1.0, 2.21529, and 4.63963 days, respectively. Their radii and masses are 1.5, 3.0, and $7 R_{\oplus}$, and 5, 10, and $62 M_{\oplus}$, respectively. The orbits of the two innermost planets are circular, whereas the outer planet has a non-zero eccentricity of $e_c = 0.1$ with the star's argument of periastron $\omega_{\star,c} = 204$ deg. We assumed inclinations of $i_b = 87$ deg, $i_c = 88$ deg, and $i_d = 84$ deg, so that the two innermost planets transit the star while planet d does not. We assumed that gravitational interaction between the three planets is negligible. We imposed limb darkening coefficients of $u_1 = 0.43$ and $u_2 = 0.31$. We used these values to calculate the scaled parameters used by `pyaneti`. Details of the whole set of fitted parameters are given in Table 1.

The synthetic light curve covers a range of 30 days starting at an arbitrary 0 point. We created the instantaneous normalized flux due to the transiting planets using eq. (24) with continuous time stamps separated by 5 minutes. We added Gaussian noise at the 5×10^{-5} level to simulate high precision photometry, such as that provided by `Kepler`. The synthetic light curve is displayed in the upper panel of Fig. 3.

The simulated RV measurements cover the 30 days simultaneous to the light curve data. Time stamps were taken from a random uniform distribution and the corresponding RVs were calculated using eq. (19). We simulated data for two spectrographs called instrument A and B. For spectrograph A, we created 50 absolute RVs with Gaussian noise of 1 m s^{-1} assuming a systemic velocity of 10 km s^{-1} . For instrument B, we simulated 50 time stamps with Gaussian noise of 5 m s^{-1} , but we assigned error bars of 3 m s^{-1} to each point to simulate a jitter term of $\sigma_j = (5^2 - 3^2)^{1/2} \text{ m s}^{-1} = 4 \text{ m s}^{-1}$. We assumed that the RVs of instrument B are relative and arbitrarily centered around 0 km s^{-1} . The lower panel of Fig. 3 shows the synthetic data-points following the correction for the RV offset between the two instruments.

We performed a joint fit setting uniform priors for all the parameters (details are given in Table 1). We used 100 independent Markov chains started randomly inside the uniform prior ranges. Once all chains converged, we used the last 5000 iterations and saved the chains' states every 10 iterations. This approach generated a posterior distribution of 50,000 points for each parameter.

5.1.2 Results

Table 1 contains the medians and 68% credible intervals of the posterior distributions of the fitted parameters. We note that the system parameter's true values are inside the posterior distribution of each parameter. In most cases, the true values are inside the 68% credible interval. This shows the power of `pyaneti` to infer real parameters from data.

The lower panel of Fig. 3 shows the simulated RV data and the inferred best-fitting three-planet model. Figure 4 displays the phase-folded transit and RV curves. Figure 5 displays the posterior distributions of some of the fitted parameters. These histograms are useful diagnostic plots to check the goodness of the MCMC output. We note that our analysis provides unimodal posterior distributions. Their shapes are either Gaussian ($T_{0,b}$ and P_b), or skewed ($\rho_{\star}^{1/3}$ and $R_{p,c}/R_{\star}$). The 68% credible intervals are over plotted on

⁴ More documentations are available at <http://www.f2py.com/>.


```

input : RV and/or light curve time-series, correct input file for star-name
output: Posterior distributions, plots, parameter inference of RV and/or transit models from data

1 ./pyaneti.py star-name (start of the run)
2 Read initial files (functions, default values)
3 Read input file with parameters for the current run (number of planets, priors, flags)
4 Read time-series data
5 Pass data and variables to FORTRAN routines
6 Start FORTRAN execution
7 Create random chains inside the prior ranges
8 Calculate likelihoods and priors for the initial state
9 Set iteration control variable continua to True
10 Initialize iterations count variable i=0
11 while continua do
12     Evolve chains following Algorithm 1                                ! This line can also run in parallel
13     check for convergence after  $N$  iterations                       !  $N$  is calculated as niter  $\times$  thin_factor
14     if i ==  $N$  then
15         Check convergence using Gelman & Rubin (1992) criteria
16         if chains converged == False then
17             continua = True                                       !Chains have not converged: Keep iterating
18             i = 0                                                    ! restart iteration counter
19         else
20             continua = False                                       !Chains have converged: save posteriors
21         end
22     end
23 end
24 Write posterior distributions with the converged chains taking into account the thin factor
25 End of FORTRAN execution
26 Run PYTHON output routines
27 Read posterior from posterior file
28 Automatic calculation of parameters and creation of plots
29 Save data in the outpy/star-name_out directory
30 End of run for star-name

```

Algorithm 2: General algorithm of *pyaneti*.

each histogram; they corresponds to the error bars reported in Table 1.

We note that the jitter term of instrument B found by *pyaneti* ($\sigma_B = 4.09^{+0.77}_{-0.68}$ m s⁻¹; cfr. Table 1) agrees with the simulated value of 4 m s⁻¹. We stress that jitter terms must be used when we have a reason to believe that the error bars are underestimated ($\chi^2/\text{dof} > 1$). If a fit is poor, it is recommended to first check if the model can be improved before adding a jitter term. The derived stellar density is fully consistent with the density expected for the simulated host star. We emphasize that *pyaneti* fits for the stellar mean density instead for the scaled semi-major axis of planet b and c (see Sect. 3.4).

5.2 The multi-planet system K2-38

5.2.1 Setup

We also tested *pyaneti* with a real planetary system. We modeled the transit photometry and radial velocities of K2-38 and compared our results with those published by Sinukoff et al. (2016). K2-38 is G2 V star transited by two planets whose masses have been measured via Doppler spectroscopy. The inner planet, K2-38 b, orbits the star every 4 days. It has a mass of 12 M_\oplus and a radius of 1.55 R_\oplus .

The outer transiting planet, K2-38 b, has an orbital period of 10.5 days, a mass of 9.8 M_\oplus , and a radius of 2.4 R_\oplus .

K2-38 was photometrically observed by the K2 mission (Howell et al. 2014) during its campaign 2. The RV measurements were gathered with the HIRES spectrograph (Vogt et al. 1994) mounted at the Keck I 10 m telescope, at Keck Observatory (Mauna Kea, Hawai'i). Sinukoff et al. (2016) detected a linear trend in the RV measurements, indicative of the presence of an additional companion in the system. While modeling the RV data, the authors added a jitter term to the nominal uncertainties to account for instrumental velocity noise not included in the nominal uncertainties and/or possible sources of stellar variability. Because of its complexity, this system is an ideal test-bench for *pyaneti*.

We used the EVEREST processed light curve (Luger et al. 2016) to perform the transit light curve analysis. We de-trended the K2 data with *extrending* (Barragán & Gandolfi 2017) by fitting a second-order polynomial function to the 5-hour out-of-transit data centered around each transit. The RV measurements were taken from Sinukoff et al. (2016).

We used the general form of the likelihood given in eq. (3) to account for the RV jitter term. We added a linear trend term $\dot{\gamma}$ to equation (19) taking as zero point the time of conjunction of planet b. We super-sampled the transit model by a factor of 10 to account for the K2 long-cadence

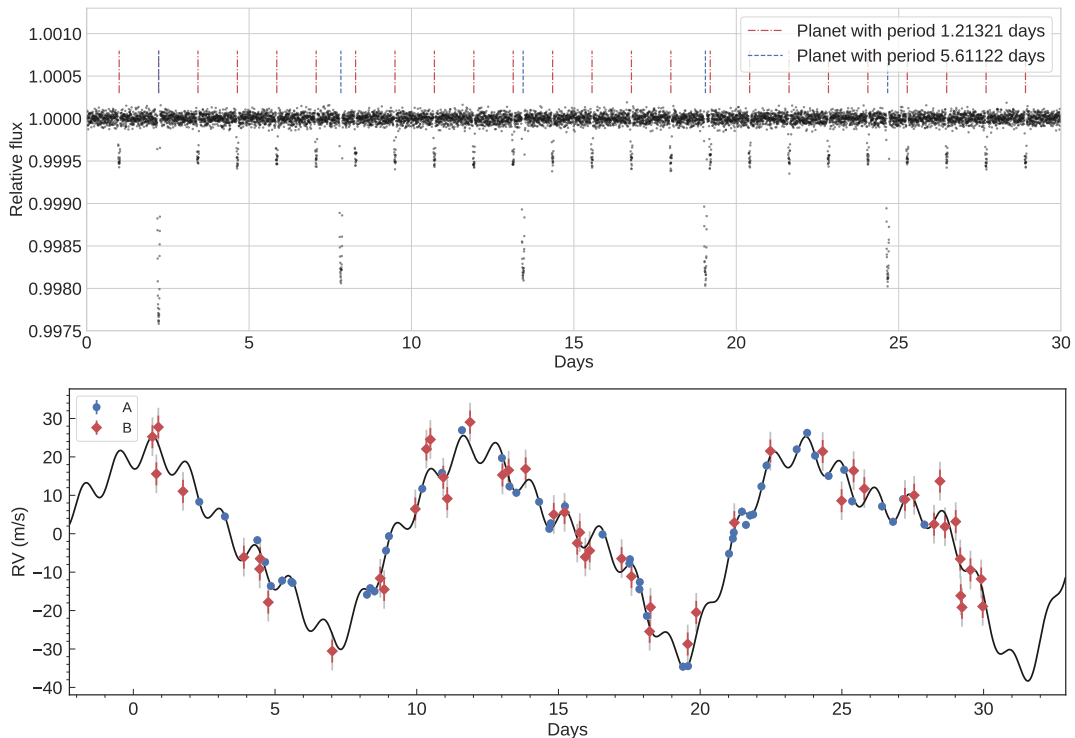


Figure 3. *Upper panel:* Thirty-day-long synthetic light curve. We assumed a relative flux of 1 with no trends. There are two transiting planets with different periods and sizes, marked with dashed lines. *Lower panel:* Synthetic RV measurements. The RV signal consists of three planets with different masses and periods. Instrument A (blue circles) has a precision of 1 m s^{-1} , whereas instrument B (red squares) has a precision of 5 m s^{-1} . The nominal error bars of instrument B were set to 3 m s^{-1} to simulate a jitter term (gray extensions to the nominal error bars). The best fitting model is shown as a thick black line. Offsets were subtracted to both data sets.

data (Kipping 2013). We fixed q_2 to 0.5 to recover the linear limb darkening case and set **Gaussian** priors on q_1 with $1\text{-}\sigma$ uncertainty of 0.1. We set uniform priors for the remaining parameters (details are provided in Table 2) and assumed circular orbits as adopted by Sinukoff et al. (2016). The sampling of the parameter space follows the procedure described in Sect. 5.1. Briefly, we initialized 100 independent chains created randomly inside the prior ranges. Once all chains converged, we created posterior distributions with 50,000 independent points for each parameter.

5.2.2 Results

The final estimates and their $1\text{-}\sigma$ uncertainties are taken as the median and the 68% of the credible interval of the posterior distributions. Values are reported in Table 2. Photometric and RV data, along with the best fitting transit and RV models are displayed in Figure 6.

We compare our results with those from Sinukoff et al. (2016) in Table 2. The parameter estimates agree well within their $1\text{-}\sigma$ uncertainties. However, we note that the largest discrepancies are found for the parameters derived from the K2 data. This is very likely due to the different extracted light curve used in our analysis, as well as on the different transit de-trending algorithm. As for the RV-derived parameters, our results are in excellent agreement with those reported by Sinukoff et al. (2016).

This test confirms the correct **implementation** of the MCMC method and multiplanet equations. Sinukoff et al.

(2016) used the widely used ensemble sampler package **emcee** (Foreman-Mackey et al. 2013).

5.3 Execution performance

We show here that **pyaneti** is able to produce scientific results within a few minutes in a personal laptop. We ran the test case presented in section 5.2 (2 planet system, 435 data points, 10 000 iterations with 100 independent Markov chains) with different CPU configurations. We used a machine with an Intel i7-6500U CPU (Four 2.50GHz cores) and with Linux (Fedora 64-bit) operating system. We compiled the code with **gfortran** 8.1.1 and used 1, 2, and 4 CPUs. The respective execution times were 10m 11s, 5m 56s and 4m 22s. These results prove the power of the code to perform a full run in a personal laptop. However, we stress that the execution time depends on the analyzed data set. Based on our experience with **pyaneti**, the modeling of only RV data is carried within a few minutes. For demanding fits requiring longer execution time (e.g., long time-series photometry), **pyaneti** can be ran in parallel in a server machine equipped with more than one CPU.

6 CONCLUSIONS

We have developed and tested the code **pyaneti**, a software suite able to simultaneously fit RV and transit light curves of multi-planet systems. **pyaneti** combines the computational

Table 1. System parameters.

Parameter	Real value	Prior ^(a)	Inferred value
<i>Model Parameters planet b</i>			
Orbital period P_{orb} (days)	1.21321	$\mathcal{U}[1.2122, 1.2142]$	1.2132028 ± 0.0000097
Transit epoch T_0	1.0	$\mathcal{U}[0.9965, 1.0035]$	1.00010 ± 0.00012
Scaled planet radius R_p/R_\star	0.020525	$\mathcal{U}[0, 0.1]$	$0.0204479^{+0.00027}_{-0.00015}$
Impact parameter, b	0.33	$\mathcal{U}[0, 1]$	$0.25^{+0.13}_{-0.15}$
e	0	$\mathcal{F}[0]$	0
ω_\star	0	$\mathcal{F}[0]$	0
Radial velocity semi-amplitude variation K (m s^{-1})	3.95	$\mathcal{U}[0, 50]$	4.16 ± 0.23
<i>Model Parameters planet c</i>			
Orbital period P_{orb} (days)	5.61122	$\mathcal{U}[5.6012, 5.6212]$	5.611254 ± 0.000041
Transit epoch T_0	2.21529	$\mathcal{U}[2.2143, 2.2163]$	2.21530 ± 0.00010
Scaled planet radius R_p/R_\star	0.04105	$\mathcal{U}[0, 0.1]$	$0.04058^{+0.00057}_{-0.00030}$
Impact parameter, b	0.60	$\mathcal{U}[0, 1]$	$0.57^{+0.06}_{-0.03}$
e	0	$\mathcal{F}[0]$	0
ω_\star	0	$\mathcal{F}[0]$	0
Radial velocity semi-amplitude variation K (m s^{-1})	4.74	$\mathcal{U}[0, 50]$	4.86 ± 0.33
<i>Model Parameters planet d</i>			
Orbital period P_{orb} (days)	12.12349	$\mathcal{U}[11.8235, 12.4235]$	12.142 ± 0.028
Transit epoch T_0	4.640	$\mathcal{U}[4.1396, 5.1396]$	4.592 ± 0.052
e	0.1	$\mathcal{U}[0, 1]$	0.096 ± 0.012
ω_\star	3.57	$\mathcal{U}[0, 2\pi]$	3.60 ± 0.14
Radial velocity semi-amplitude variation K (m s^{-1})	22.75	$\mathcal{U}[0, 50]$	22.99 ± 0.24
<i>Other Parameters</i>			
Cubic root of stellar density $\rho_\star^{1/3}$	1.458	$\mathcal{U}[0.05, 2]$	$1.496^{+0.039}_{-0.072}$
Systemic velocity γ_A (km s^{-1})	10	$\mathcal{U}[9, 11]$	9.99991 ± 0.00017
Systemic velocity γ_B (km s^{-1})	0	$\mathcal{U}[-1, 1]$	0.00107 ± 0.00084
Jitter term σ_A (m s^{-1})	0	$\mathcal{U}[0, 100]$	$0.25^{+0.24}_{-0.18}$
Jitter term σ_B (m s^{-1})	4	$\mathcal{U}[0, 100]$	$4.09^{+0.77}_{-0.68}$
Parameterized limb-darkening coefficient q_1	0.55	$\mathcal{U}[0, 1]$	0.60 ± 0.05
Parameterized limb-darkening coefficient q_2	0.29	$\mathcal{U}[0, 1]$	$0.25^{+0.05}_{-0.04}$

Note – ^(a) $\mathcal{U}[a, b]$ refers to uniform priors between a and b and $\mathcal{F}[a]$ to a fixed value a .

power of FORTRAN with the versatility of PYTHON and it offers the option to run in parallel with OpenMP. The package has been developed under “the open source ideology”, i.e., both the code and the platforms used to write the package are totally free.

We have tested pyaneti with synthetic data and proved that the code is able to recover the parameters of multi-planet systems. We have also performed an independent fit of K2-38 and our results are consistent with those in the literature. The joint modeling of the transit and RV measurements of the K2-38 system takes only ~5 min on a personal laptop. This demonstrates that the code can perform fast analyses and makes pyaneti a powerful tool to perform data analysis of hundreds of systems coming from future space- and ground-based instruments, such as TESS, PLATO, CHEOPS, and ESPRESSO.

Future releases of pyaneti will include extra parametric models, such as TTV, multi-band photometry and phase curves. We anticipate that the code will also be able to use other likelihoods and priors, such as Gaussian processes.

ACKNOWLEDGEMENTS

D. Gandolfi gratefully acknowledges the financial support of the *Programma Giovani Ricercatori – Rita Levi Montalcini – Rientro dei Cervelli (2012)* awarded by the Italian Ministry of Education, Universities and Research (MIUR).

REFERENCES

- Anderson D. R., et al., 2011, *ApJ*, **726**, L19
 Auvergne M., et al., 2009, *A&A*, **506**, 411
 Bakos G., Noyes R. W., Kovács G., Stanek K. Z., Sasselov D. D., Domsa I., 2004, *PASP*, **116**, 266
 Barragán O., Gandolfi D., 2017, *Exotrending*, Astrophysics Source Code Library (ascl:1706.001)
 Barragán O., et al., 2016, *AJ*, **152**, 193
 Barragán O., et al., 2018a, *MNRAS*, **475**, 1765
 Barragán O., et al., 2018b, *A&A*, **612**, A95
 Bayes M., Price M., 1763, *Philosophical Transactions (1683-1775)*, **53**, 370
 Borucki W. J., et al., 2010, *Science*, **327**, 977
 Bozza V., Mancini L., Sozzetti A., eds, 2016, *Methods of Detecting Exoplanets Astrophysics and Space Science Library Vol. 428*, doi:10.1007/978-3-319-27458-4.
 Broeg C., et al., 2013, in *European Physical Journal*

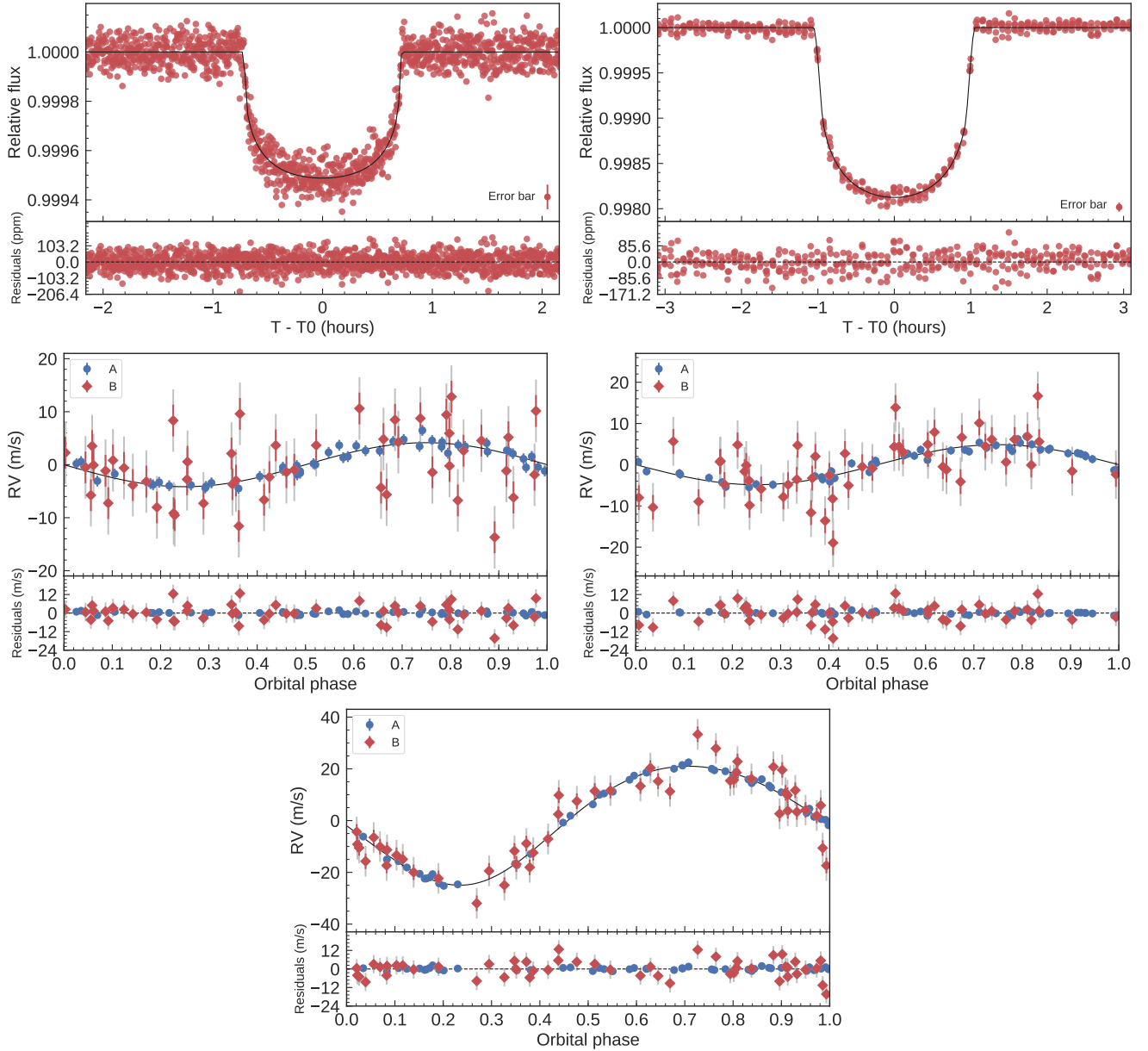


Figure 4. *Upper panels:* Phase-folded light curves for planet b and c of the simulated planetary system. Synthetic data points are plotted with the red circles. The best fitting transit models are over-plotted with thick black lines. *Middle and lower panels:* Phase-folded RV curves for planet b, c and d of the simulated planetary model. Synthetic data for instrument A is shown with blue circles, whereas for instrument B with red diamonds. The best fitting RV models are over-plotted with thick black lines. The gray error bars account for the jitter term for each instrument.

Web of Conferences. p. 03005 ([arXiv:1305.2270](https://arxiv.org/abs/1305.2270)), [doi:10.1051/epjconf/20134703005](https://doi.org/10.1051/epjconf/20134703005)
 Chakraborty A., Roy A., Sharma R., Mahadevan S., Chaturvedi P., Prasad N. J. S. S. V., Anandarao B. G., 2018, *AJ*, **156**, 3
 Charbonneau D., Brown T. M., Latham D. W., Mayor M., 2000, *ApJ*, **529**, L45
 Christen J., 2007, Technical Report I-07-16, CIMAT, Guanajuato
 Claret A., Bloemen S., 2011, *A&A*, **529**, A75
 Cosentino R., et al., 2012, in *Ground-based and Airborne Instrumentation for Astronomy IV*. p. 84461V, [doi:10.1117/12.925738](https://doi.org/10.1117/12.925738)
 Csizmadia S., et al., 2015, *A&A*, **584**, A13
 Díaz R. F., 2018, *Asteroseismology and Exoplanets: Listening to the Stars and Searching for New Worlds*, **49**, 199

Donati J.-F., Kouach D., Lacombe M., Baratchart S., Doyon R., Delfosse X., et al. 2017, SPIRou: A nIR Spectropolarimeter/High-precision Velocimeter for the CFHT. p. 107, [doi:10.1007/978-3-319-30648-3_107-1](https://doi.org/10.1007/978-3-319-30648-3_107-1)
 Eastman J., Gaudi B. S., Agol E., 2013, *PASP*, **125**, 83
 Foreman-Mackey D., Hogg D. W., Lang D., Goodman J., 2013, *PASP*, **125**, 306
 Fridlund M., et al., 2017, *A&A*, **604**, A16
 Gandolfi D., et al., 2017, *AJ*, **154**, 123
 Gelman A., Rubin D. B., 1992, *Statistical Science*, **7**, 457
 Gelman A., Carlin J. B., Stern H. S., Rubin D. B., 2004, *Bayesian Data Analysis*, 2nd ed. edn. Chapman and Hall/CRC
 Gillon M., et al., 2017, *Nature*, **542**, 456
 Goodman J., Weare J., 2010, *Commun Appl Math Comput Sci*,

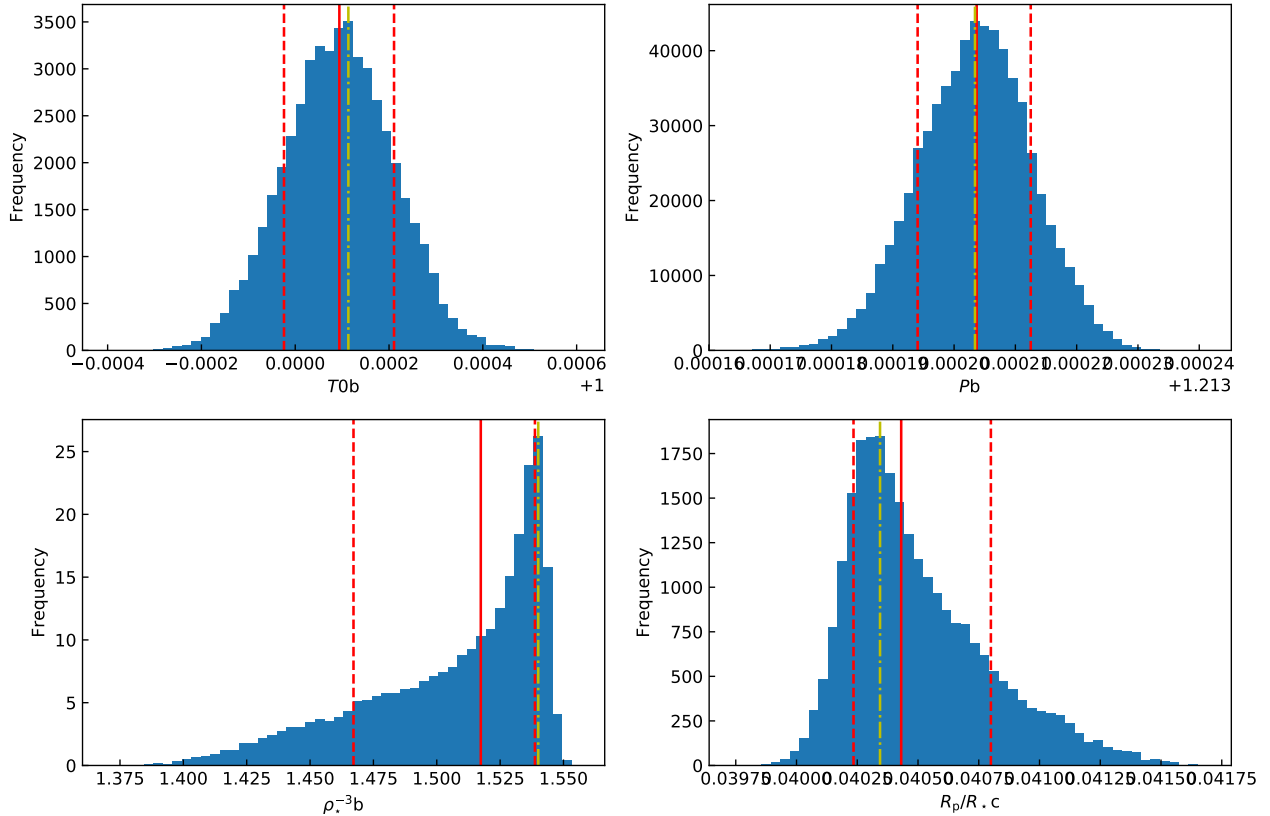


Figure 5. Posterior distributions for $T_{0,b}$ (upper left), P_b (upper right), ρ_*^{-3b} (lower left), and $R_{p,c}/R_*$ (lower right) of the toy model fit. The solid red lines mark the medians of the distributions, whereas the dashed red lines mark the limits of the 68% credible intervals. The mode are shown with the dot-dashed yellow lines.

5, 65
 Guenther E. W., et al., 2017, *A&A*, **608**, A93
 Hastings W. K., 1970, *Biometrika*, **57**, 97
 Hatzes A. P., et al., 2011, *ApJ*, **743**, 75
 Henry G. W., Marcy G., Butler R. P., Vogt S. S., 1999, *IAU Circ.*, **7307**
 Hogg D. W., Foreman-Mackey D., 2018, *ApJS*, **236**, 11
 Hou F., Goodman J., Hogg D. W., Weare J., Schwab C., 2012, *ApJ*, **745**, 198
 Howell S. B., et al., 2014, *PASP*, **126**, 398
 Juvan I. G., Lendl M., Cubillos P. E., Fossati L., Tregloan-Reed J., Lammer H., Guenther E. W., Hanslmeier A., 2018, *A&A*, **610**, A15
 Kipping D. M., 2010, *MNRAS*, **408**, 1758
 Kipping D. M., 2013, *MNRAS*, **435**, 2152
 Li Y., Stefansson G., Robertson P., Monson A., Cañas C., Mahadevan S., 2017, *Research Notes of the American Astronomical Society*, **1**, 49
 Livingston J. H., et al., 2018, preprint, ([arXiv:1806.11504](https://arxiv.org/abs/1806.11504))
 Lucy L. B., Sweeney M. A., 1971, *AJ*, **76**, 544
 Luger R., Agol E., Kruse E., Barnes R., Becker A., Foreman-Mackey D., Deming D., 2016, *AJ*, **152**, 100
 Mandel K., Agol E., 2002, *ApJ*, **580**, L171
 Mayor M., Queloz D., 1995, *Nature*, **378**, 355
 Mayor M., et al., 2003, *The Messenger*, **114**, 20
 Metropolis N., Rosenbluth A. W., Rosenbluth M. N., Teller A. H., Teller E., 1953, *J. Chem. Phys.*, **21**, 1087
 Murray C. D., Correia A. C. M., 2010, *Keplerian Orbits and Dynamics of Exoplanets*. pp 15–23
 Parviainen H., 2015, *MNRAS*, **450**, 3233
 Parviainen H., 2017, *Bayesian Methods for Exoplanet Science*. p. 149, [doi:10.1007/978-3-319-30648-3_149-1](https://doi.org/10.1007/978-3-319-30648-3_149-1)
 Pepe F. A., et al., 2010, in *Ground-based and Airborne Instrumentation for Astronomy III*. p. 77350F, [doi:10.1117/12.857122](https://doi.org/10.1117/12.857122)
 Pepper J., et al., 2007, *PASP*, **119**, 923
 Perryman M., 2011, *The Exoplanet Handbook*
 Pollacco D. L., et al., 2006, *PASP*, **118**, 1407
 Prša A., et al., 2016, *AJ*, **152**, 41
 Rauer H., et al., 2014, *Experimental Astronomy*, **38**, 249
 Ricker G. R., et al., 2015, *Journal of Astronomical Telescopes, Instruments, and Systems*, **1**, 014003
 Sanchis-Ojeda R., Rappaport S., Winn J. N., Kotson M. C., Levine A., El Mellah I., 2014, *ApJ*, **787**, 47
 Seager S., 2010, *Exoplanets*
 Seager S., Mallén-Ornelas G., 2003, *ApJ*, **585**, 1038
 Sharma S., 2017, *ARA&A*, **55**, 213
 Sinukoff E., et al., 2016, *ApJ*, **827**, 78
 Vogt S. S., et al., 1994, in *Crawford D. L., Craine E. R., eds, Proc. SPIE Vol. 2198, Instrumentation in Astronomy VIII*. p. 362, [doi:10.1117/12.176725](https://doi.org/10.1117/12.176725)
 Winn J. N., 2010, *Exoplanet Transits and Occultations*. University of Arizona Press, pp 55–77
 Wright J. T., Howard A. W., 2009, *ApJS*, **182**, 205

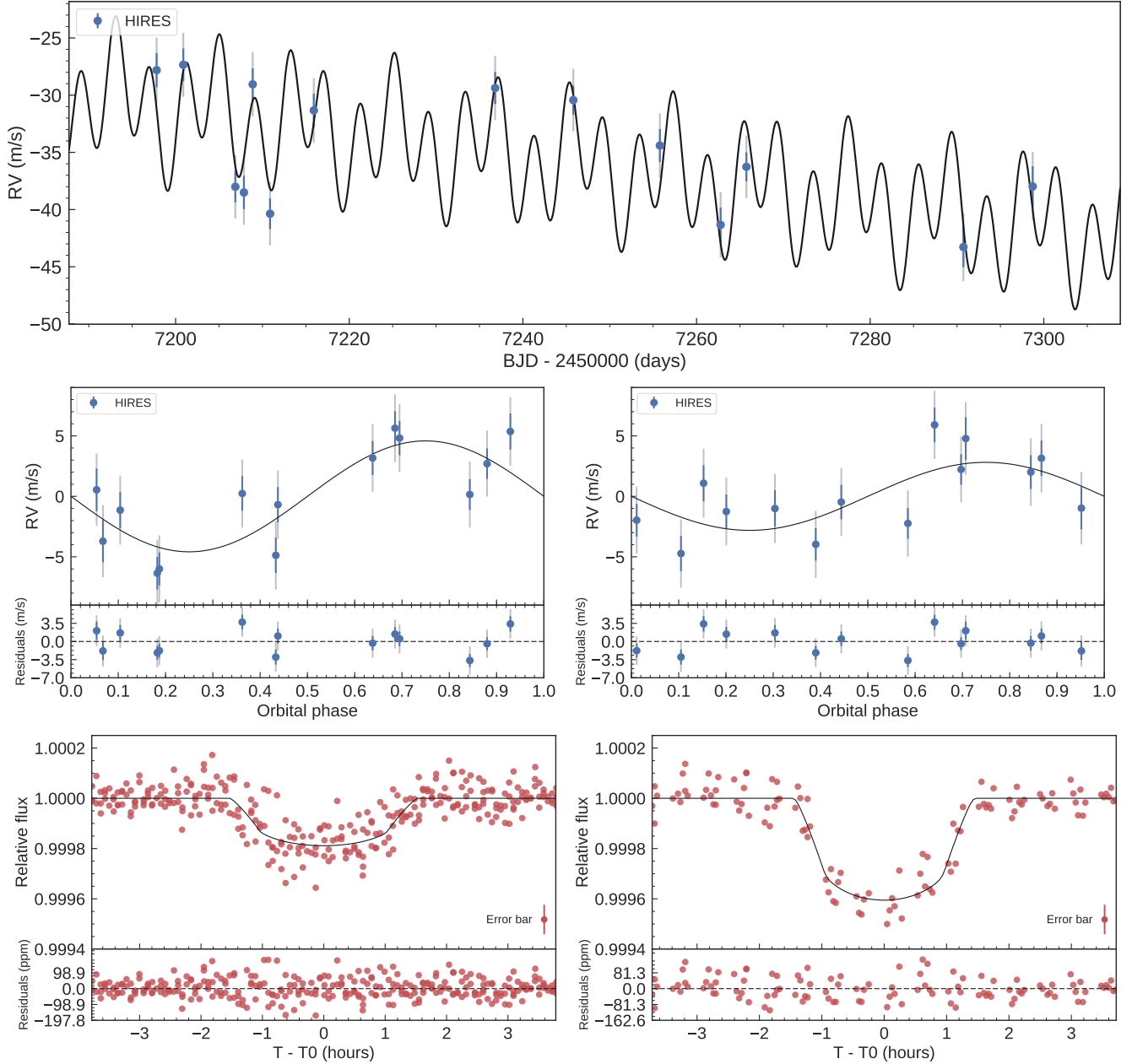


Figure 6. *Upper panel:* Hires RV measurements of K2-38 (blue circles). The best-fitting solution is shown with a thick black line. A linear trend is visible in the data. The fitted stellar jitter is shown as a gray extension to the nominal error bars. *Middle panels:* Phase-folded RV curves for K2-38 b (left) and K2-38 c (right). *Lower panels:* Transit light curve folded to the orbital period of K2-38 b (left) and K2-38 c (right), and residuals. The red points are K2 data. The thick black lines mark the best fitting transit models.

APPENDIX A: NUMERICAL TREATMENT OF THE POSTERIOR

Equation (4) may lead to very small/big numbers which generate numerical overflows. Therefore it is convenient to use the logarithmic of probability densities. Bayes' theorem is rewritten as

$$\ln P(M|D) = \ln P(D|M) + P(M) - P(D). \quad (\text{A1})$$

We note that this treatment of the posterior does not

affect the MCMC method. Since the ratio between the actual and proposed states can be calculated easily as

$$\frac{P(D|\vec{\Phi})P(\vec{\Phi})}{P(D|\vec{\phi})P(\vec{\phi})} = \exp \left[\ln P(D|\vec{\Phi}) + \ln P(\vec{\Phi}) - \ln P(D|\vec{\phi}) - \ln P(\vec{\phi}) \right] \quad (\text{A2})$$

By following this approach, the general form of the

Table 2. System parameters.

Parameter	Simukoff et al. (2016)	Prior ^(a)	Fitted value
<i>Model Parameters planet b</i>			
Orbital period P_{orb} (days)	4.01593 ± 0.00050	$\mathcal{U}[4.0134, 4.0184]$	$4.01632^{+0.00032}_{-0.00034}$
Transit epoch T_0 (BJD - 2,450,000)	6896.8786 ± 0.0054	$\mathcal{U}[6896.8486, 6896.9086]$	$6896.8734^{+0.0038}_{-0.0034}$
Scaled semi-major axis a/R_{\star}	$10.7^{+1.3}_{-3.7}$	$\mathcal{U}[1.1, 50]$	$11.3^{+1.0}_{-2.3}$
Scaled planet radius R_p/R_{\star}	$0.01281^{+0.00105}_{-0.00064}$	$\mathcal{U}[0, 0.1]$	$0.01247^{+0.00087}_{-0.00045}$
Impact parameter, b	0.48 ± 0.30	$\mathcal{U}[0, 1]$	$0.35^{+0.33}_{-0.25}$
e	0	$\mathcal{F}[0]$	0
ω_{\star} (deg)	90	$\mathcal{F}[90]$	90
Radial velocity semi-amplitude variation K (m s ⁻¹)	4.6 ± 1.1	$\mathcal{U}[0, 100]$	4.6 ± 1.1
<i>Model Parameters planet c</i>			
Orbital period P_{orb} (days)	10.56103 ± 0.00090	$\mathcal{U}[10.5565, 10.5655]$	10.56155 ± 0.00049
Transit epoch T_0 (BJD - 2,450,000)	6900.4752 ± 0.0033	$\mathcal{U}[6900.4552, 6900.4952]$	6900.4740 ± 0.0018
Scaled semi-major axis a/R_{\star}	$26.3^{+5.4}_{-16.1}$	$\mathcal{U}[1.1, 50]$	$31.3^{+2.1}_{-5.1}$
Scaled planet radius R_p/R_{\star}	$0.02004^{+0.0024}_{-0.0013}$	$\mathcal{U}[0, 1]$	$0.01841^{+0.0010}_{-0.0005}$
Impact parameter, b	$0.64^{+0.23}_{-0.41}$	$\mathcal{U}[0, 1]$	$0.34^{+0.27}_{-0.25}$
e	0	$\mathcal{F}[0]$	0
ω_{\star} (deg)	90	$\mathcal{F}[90]$	90
Radial velocity semi-amplitude variation K (m s ⁻¹)	2.8 ± 1.3	$\mathcal{U}[0, 1000]$	2.8 ± 1.3
<i>Other Parameters</i>			
RV value at $T_{0,1}$ γ (m s ⁻¹) ^(b)	-1.7 ± 0.9	$\mathcal{U}[-1000, 1000]$	0.034 ± 0.010
Linear trend slope $\dot{\gamma}$ (km s ⁻¹ d ⁻¹)	-0.101 ± 0.030	$\mathcal{U}[-1, 1]$	-0.103 ± 0.029
HIRES jitter term σ_{HIRES} (m s ⁻¹)	$2.4^{+1.0}_{-0.7}$	$\mathcal{U}[0, 1000]$	$2.4^{+1.0}_{-0.7}$
Parameterized limb-darkening coefficient q_1	0.38 ± 0.1 ^(c)	$\mathcal{N}[0.38, 0.1]$	0.42 ± 0.1
Parameterized limb-darkening coefficient q_2	0.5 ^(c)	$\mathcal{F}[0.5]$	0.5

Note – ^(a) $\mathcal{U}[a, b]$ refers to uniform priors between a and b , $\mathcal{N}[a, b]$ to Gaussian priors with median a and standard deviation b , and $\mathcal{F}[a]$ to a fixed value a . ^(b) Our results and Simukoff et al. results do not agree because the instant at which the intercept is calculated is not the same. ^(c) We transform the values reported by Simukoff et al. to the q_1 and q_2 parametrization to perform the comparison.

Gaussian likelihood for an RV and transit fit is given using eq. (4) as

$$P(D|M) = \prod_i^{N_{\text{RV}}} \left[\frac{1}{\sqrt{2\pi(\sigma_i^2 + \sigma_j^2)}} \right]_{\text{RV}} \times \prod_i^{N_{\text{LC}}} \left[\frac{1}{\sqrt{2\pi(\sigma_i^2 + \sigma_j^2)}} \right]_{\text{LC}} \times \exp \left\{ -\frac{1}{2} \chi_{\text{Tot}}^2 \right\}, \quad (\text{A3})$$

where

$$\chi_{\text{Tot}}^2 = \sum_i^{N_{\text{RV}}} \frac{(D_{i,\text{RV}} - M_{i,\text{RV}})^2}{\sigma_i^2 + \sigma_j^2} + \sum_i^{N_{\text{LC}}} \frac{(D_{i,\text{LC}} - M_{i,\text{LC}})^2}{\sigma_i^2 + \sigma_j^2}. \quad (\text{A4})$$

The RV and LC sub-indexes refers to RV and light curve data and models, respectively. The logarithmic form of the likelihood given in eq. (4) is rewritten as

$$\ln P(D|M) = -\frac{1}{2} \left[\sum_i^{N_{\text{RV}}} \ln 2\pi(\sigma_i^2 + \sigma_j^2) + \sum_i^{N_{\text{LC}}} \ln 2\pi(\sigma_i^2 + \sigma_j^2) + \chi_{\text{Tot}}^2 \right]. \quad (\text{A5})$$

We note that eq. (A5) can be used too model pure RV or transit data.

This paper has been typeset from a $\text{\TeX}/\text{\LaTeX}$ file prepared by the author.